Desalination and Water Treatment
www.deswater.com

doi: 10.5004/dwt.2019.24275

161 (2019) 92–107
September

Effect of membrane properties and operational parameters on systems for seawater desalination using computational fluid dynamics simulations

Anas M. Alwatban[a,b], Ahmed M. Alshwairekh[a,b], Umar F. Alqsair[a,c], Abdullah A. Alghafis[a,b], Alparslan Oztekin[a,*]

[a]*P.C. Rossin College of Engineering and Applied Science, Lehigh University, PA 18015, USA, Tel. +1 610 758 4343; emails: alo2@lehigh.edu (A. Oztekin), ama716@lehigh.edu (A.M. Alwatban), ama215@lehigh.edu (A.M. Alshwairekh), uma216@lehigh.edu (U.F. Alqsair), aaa614@lehigh.edu (A.A. Alghafis)*
[b]*Mechanical Engineering Department, College of Engineering, Qassim University, Qassim 52571, Saudi Arabia*
[c]*Mechanical Engineering Department, College of Engineering, Prince Sattam Bin Abdulaziz University, Alkharj 11942, Saudi Arabia*

Received 2 December 2018; Accepted 14 April 2019

ABSTRACT

Computational fluid dynamic simulations were conducted to investigate the effects of the membrane properties and operational parameters on the system performance in three-dimensional direct contact membrane distillation modules. The membrane thickness, porosity, pore size, feed flow rate, and the inlet feed temperature were considered in the parametric study. Water flux, temperature and concentration polarization characteristics of the membrane were determined. The net-type spacers were used in the feed and permeate channel to mitigate the polarization and enhance the flux performance of the separation module for various flow rates. The laminar model was employed to characterize the velocity, temperature and concentration field in the empty channels and the k-ω shear stress turbulence model was employed in the module containing spacers. The permeation flux, intensity of temperature and concentration polarization increase as the thickness is reduced, and the porosity and the pore size are increased. The rate of permeation and polarizations are increased with increase in flow rate. The presence spacers enhance the membrane flux performance more than 50% and mitigate polarizations up to 30%.

Keywords: Membrane distillation; Desalination; Direct contact; Knudsen diffusion; Molecular diffusion

1. Introduction

Water demand is growing with a distressing rate as the world population increases and the irrigated agriculture expands. Water scarcity is becoming a problem in all continents with increasing demand and overused resources. Water desalination can be a sustainable solution to the water shortage concern in the world, but it is costly to build and operate large-scale desalination plants [1]. The reverse osmosis process is dominating the desalination industry [2]. There are several disadvantages of reverse osmosis process which make the process undesirable such as high fouling propensity and high operating pressures [2]. Recently, membrane distillation (MD) desalination is considered as a viable option to the reverse osmosis process [3].

MD is a thermally driven separation process where only water vapor molecules can pass through a microporous hydrophobic membrane. The driving force in the MD system is the vapor pressure difference across the membrane induced by the temperature difference between the warm feed and the cold draw solution. MD is gaining renewed attention as a promising method for water desalination since it operates under low temperatures (<90°C) which makes it easy to use waste heat or solar energy as a heat

* Corresponding author.

source [4]. Another important feature of MD process is that the membrane is less prone to potential fouling so it could be a desirable option for high concentration separation applications such as the treatment of highly contaminated water [5,6]. There are four distinct MD configurations: direct contact membrane distillation (DCMD), air gap membrane distillation, vacuum membrane distillation (VMD) and sweeping gas membrane distillation. In DCMD, the hot solution and the cold fresh water are in direct contact with the membrane surface. Evaporation takes place at the membrane pores at the feed side, vapor molecules pass through the membrane pores and condense at the permeate side over the surface of the membrane. DCMD module can be built using different membrane configurations such as flat sheets, spiral wound and hollow fiber [7]. Beside water desalination, DCMD is used in several other applications such as chemical, textile and pharmaceutical industries [7].

The schematic diagram of the DCMD module consisting of the feed and permeate channel separated by a hydrophobic membrane is shown in Fig. 1. The hot solution with a temperature T_f flows in the feed channel and the cold fresh water with a temperature of T_p flows in the permeate channel. For the fresh water production – the passage of the water vapor from the feed to the draw channel – T_f must be larger than T_p so that the vapor pressure difference across the membrane between the feed and the permeate side is positive. The operational parameters such as inlet feed temperature, inlet permeate temperature and flow rate of both streams influence the system performance. The membrane must posses certain properties so that it can perform in the desired manner. The vital membrane properties are thickness, porosity, tortuosity and pore size of the memrbane.

To date, there have been fewer CFD studies conducted on DCMD systems compared with the reverse osmosis and other membrane separation processes. Most studies on DCMD focused on the experimental investigation.

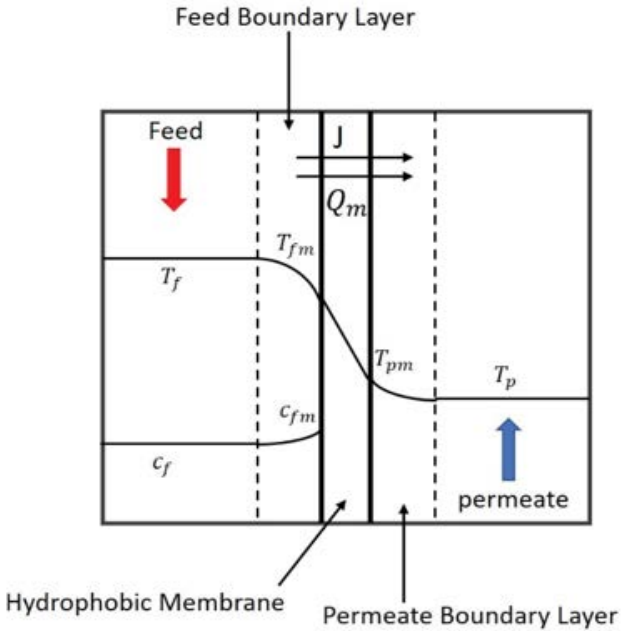

Fig. 1. Schematic diagram of the DCMD process.

Adnan et al. [8] investigated the effect of membrane support layer on the flux performance by conducting experiments in a DCMD module. They reported that the water flux was reduced by 56% when the membrane support layer is present. Bouchrit et al. [9] conducted experiments to study the capability of DCMD to treat reverse osmosis brine by using a flat-sheet membrane and showed that the DCMD could be used effectively in high concentration applications. Francis et al. [10] have measured the performance of the DCMD process for desalting seawater. The high rate of water permeation was attained for the inlet feed temperature of 80°C and the permeate temperature of 20°C. Also, they reported that the permeate flux is not sensitive to the concentration of the feed solution. Hwang et al. [11] have studied the effect of module dimensions on the DCMD flux performance using the co-current and counter-current flow modes. Their results showed that the flux obtained from two flow modes is similar, and the vapor pressure difference across the membrane decreases with the increase of the module length. Li et al. [12] studied the effect of the operating conditions on the performance of the DCMD and VMD module containing hollow fiber membranes. They reported that the permeate flux decreases in DCMD and VMD module with increasing the membrane thickness. The experimental methods provide valuable insight for DCMD systems, but it should be accompanied by CFD tools to conduct an in-depth investigation of the DCMD modules.

Yu et al. [13] conducted CFD simulations in a two-dimensional DCMD module containing a single hollow fiber. They characterized the flow and temperature field but neglected the concentration field. Yu et al. [14] have studied the effect of various operating parameters and the effect of baffles attached to the shell wall. They concluded that the temperature polarization coefficient decreases as the permeability increases and that the baffles improve the flux performance for the high permeability membranes at high flow rates. Yang et al. [15] conducted CFD simulations to investigate the effect of microstructure of the hollow fibers on the membrane performance by considering various patterned micro-sized corrugations over the hollow fiber membrane. They have characterized the temperature variation along the membrane but neglected the concentration variations. The membrane was treated as an impermeable surface in their study. Al-Sharif et al. [16] have performed numerical analyses to study the effects of spacers on the heat transfer enhancement in DCMD systems by considering various types of innovative spacer design. Hayer et al. [17] conducted simulations in a two-dimensional DCMD module to determine the velocity, temperature and concentration field. They reported that the permeate flux is strongly influenced by the membrane thickness and the inlet feed temperature, but it is hardly affected by the concentration of the feed solution. Computational fluid dynamics simulations conducted by Chang et al. [18] considered DCMD systems containing rough and flat channels. The temperature and the concentration field were characterized, and the membrane permeability was calculated based on Knudsen, molecular, and viscous diffusion. Park et al. [19] simulated the desalination process in a two-dimensional DCMD module to characterize the flow, temperature and concentration field. The effects of the operating parameters

on the flux performance of the module were investigated. They concluded that the water permeation rate and the intensity of temperature polarization increases as the inlet feed temperature is increased. Soukane et al. [20] performed a computational study for water desalination process in three-dimensional DCMD modules. Flow simulations were conducted in the feed channel, and the effect of the permeate channel was included through boundary conditions imposed on temperature, concentration and velocity field. They have considered two membranes with different thickness, pore size and porosity, and concluded that the temperature polarization effects are dominant at all inlet feed temperatures.

Hitsov et al. [21] documented an extensive review of the mathematical modeling for the membrane distillation process. They stated that even though the MD process was discovered over 50 years ago, commercialized industrial-scale MD desalination modules have not been developed and deployed. They recommended that the MD community must have an in-depth understanding of the transport phenomena inside the channels and through the membrane. This detailed understanding could be provided by combined experimental measurements and CFD simulations utilizing accurate mathematical modeling. There were only a few previous CFD investigations as presented and discussed above. Many of these studies have omitted some aspects of important physical phenomenon involved in MD systems by overly simplifying the model or the geometry. It is imperative to carry out more computational studies to better understand MD systems so that MD separation process can become a competitive technology.

This work aims to develop an accurate CFD model that can capture most of the critical details in three-dimensional DCMD systems. The current work focusses on systematically studying the effect of membrane properties and feed operational parameters. The membrane properties are essential to the understanding of the DCMD separation process, and they should be included in the design and optimization of these modules [22]. The membrane permeability, determined based on the Knudsen and molecular diffusion, is taken as a function of both membrane properties and operational parameters. The effects of the net-type of spacers on the membrane flux performance and membrane polarization characteristics are investigated. The three-dimensional CFD model developed in this work adds more insight into the heat and mass transfer phenomenon involved in DCMD systems and should be used as a guide in selecting the proper membrane permeability and the optimum operating parameters of DCMD systems.

2. Mathematical model

Three-dimensional steady state incompressible flows are considered in the feed and the permeate channel. The conservation of mass is written as follows:

$$\nabla \cdot \vec{U} = 0 \tag{1}$$

The momentum equation is as follows:

$$\vec{U} \cdot \nabla \vec{U} = \frac{1}{\rho}\left[-\nabla p + \nabla \cdot \left(\mu \nabla \vec{U}\right)\right] \tag{2}$$

The equations governing the solute mass and energy transport are described by the equation as follows:

$$\left(\vec{U} \cdot \nabla\right) c = D\nabla^2 c \tag{3}$$

$$\vec{U} \cdot \nabla T = \frac{k_f}{\rho c_p}\nabla^2 T \tag{4}$$

Here ρ is the density, p is the pressure, μ is the viscosity, c is the solute mass fraction, D is the solute diffusion coefficient, T is the temperature, k_f is the thermal conductivity of the solution, c_p is the specific heat of the water and $\vec{U}$ is the velocity vector. The fluid viscosity is taken as a function of temperature and salt mass fraction

$$\mu = 0.001 \ln\left(-3.79418 + \frac{604.129}{139.18 + T}\right)\left(1 + A_\mu c + B_\mu c^2\right) \tag{5}$$

Eq. (5) is valid for the temperature ranging from 20°C to 180°C and for the salinity ranging from 0 to 130 g kg^{-1} [23,24]. Here $A_\mu = 1.474 \times 10^{-3} + 1.5 \times 10^{-6}T - 3.927 \times 10^{-8}T^2$ and $B_\mu = 1.073 \times 10^{-5} - 8.5 \times 10^{-8}T + 2.23 \times 10^{-10}T^2$ are temperature-dependent functions.

The equations (1)–(4) are used to simulate laminar flows in the empty module while the SST k-ω turbulence model equations are used to simulate flows in the module containing spacers. The SST k-ω turbulence momentum mass and energy equation:

$$u_j \frac{\partial u_i}{\partial x_j} = -\frac{1}{\rho}\frac{\partial p}{\partial x_i} + \frac{1}{\rho}\frac{\partial}{\partial x_j}\left(\left(\mu + \mu_t\right)\frac{\partial u_i}{\partial x_j}\right) \tag{6}$$

$$u_j \frac{\partial c}{\partial x_j} = \frac{\partial}{\partial x_j}\left(\left(D + \frac{\mu_t}{\rho \mathrm{Sc}_t}\right)\frac{\partial c}{\partial x_j}\right) \tag{7}$$

$$u_j \frac{\partial T}{\partial x_j} = \frac{\partial}{\partial x_j}\left(\left(\frac{k_f}{\rho c_p} + \frac{\mu_t}{\rho \mathrm{Pr}_t}\right)\frac{\partial T}{\partial x_j}\right) \tag{8}$$

Here, Sc_t is the turbulent Schmidt number, Pr_t is the turbulent Prandtl number and $\mu_t = \rho\frac{a_1 k}{\max\left(a_1\omega, SF_2\right)}$ is the eddy viscosity. The turbulent kinetic energy k and the specific dissipation rate ω are given as follows:

$$u_i \frac{\partial\left(\rho k\right)}{\partial x_i} = \tau_{ij}\frac{\partial u_i}{\partial x_j} - \beta^*\rho\omega k + \frac{\partial}{\partial x_j}\left(\left(\mu + \sigma_k \mu_t\right)\frac{\partial k}{\partial x_j}\right) \tag{9}$$

$$u_i \frac{\partial\left(\rho\omega\right)}{\partial x_i} = \frac{\gamma}{\nu_t}\tau_{ij}\frac{\partial u_i}{\partial x_j} - \beta\rho\omega^2 + \frac{\partial}{\partial x_j}\left[\left(\mu + \sigma_\omega \mu_t\right)\frac{\partial \omega}{\partial x_j}\right] + 2\rho\left(1 - F_1\right)\sigma_{\omega 2}\frac{1}{\omega}\frac{\partial k}{\partial x_j}\frac{\partial \omega}{\partial x_j} \tag{10}$$

where S is the vorticity magnitude, γ, a_1, β, β*, σ_k, σ_ω and $\sigma_{\omega 2}$ are the closure coefficients, and F_1, F_2 are the blending

functions. Details of the closure coefficients and blending functions can be found in the study by Menter [25].

The water flux (J) in the MD process is a function of the vapor pressure difference across the membrane, and it is calculated by the following equation [21]:

$$J = C\left(P_{v,f} - P_{v,p}\right) \tag{11}$$

$P_{v,f}$, $P_{v,p}$ are the vapor pressure of the feed and the permeate solution at the membrane surface, respectively. They are determined as a function of local temperature and concentration using the modified Antoine equation [20] as follows:

$$P_v = \frac{\exp\left(23.1964 - \frac{3816.44}{T - 46.13}\right)}{1 + 0.57357\left(\frac{c}{1000 - c}\right)} \tag{12}$$

where c is in the unit of g kg^{-1}. C, the membrane permeability, is obtained based on the dusty gas model (DGM) [21,26,27]. The DGM describes the diffusion inside the membrane to occur by a combination of several mechanisms. These mechanisms are Knudsen, molecular and viscous diffusion. The viscous diffusion could be neglected in DCMD module since the difference in the total pressure across the membrane is small. The Knudsen number, Kn = λ/d_p, determines the diffusion resistance that dominates the mass transport through the membrane. Here $\lambda = \left(K_B T\right) \Big/ \sqrt{2}\pi \bar{P} \sigma^2$ is the mean free path, d_p is the membrane pore diameter, K_B is the Boltzmann constant, T is the inlet feed temperature, $\bar{P}$ is the average pressure across the membrane pores and σ^2 is the collision diameter of water. The Knudsen diffusion (C_K) is used to describe the membrane permeability when the mean free path of water vapor molecule is larger than the membrane pore diameter (Kn > 1). In this regime, collisions of molecules with the pore wall dominate the vapor transport through the membrane. The molecular diffusion (C_m) is considered as a membrane permeability when the membrane pore diameter is much larger than the mean free path of water vapor molecule (Kn < 0.01). In this regime, the trapped air within the membrane pore adds resistance to the movement of vapor molecules, and collisions of molecules with the pore walls can be ignored. In the transition regime (0.01 < Kn < 1), the combined Knudsen and the molecular diffusion (C_{K+m}) are used to describe the membrane permeability. Table 1 shows the three models used for determining the membrane permeability [21,27–29].

Here, δ is the membrane thickness, τ is the membrane tortuosity, r is the membrane pore radius, ε is the membrane porosity, R is the universal gas constant, $T_{\text{ave}} = \frac{T_{\text{fm}} + T_{\text{pm}}}{2}$ is the average temperature inside the membrane pore, T_{fm} is the temperature at the feed side, T_{pm} is the temperature at the permeate side, M_w is the molecular weight of water, P_a, the partial pressure of air, is taken as the atmospheric pressure [30], and $\text{PD}_v = 1.895 \times 10^{-5} T^{2.072}$ is the product of the total pressure and the diffusion coefficient of vapor [30,31].

Table 1
Permeability models

Knudsen number	Mass transfer coefficient equation
Kn > 1	$C_{K=} \frac{2r\varepsilon}{3\delta\tau}\sqrt{\frac{8M_w}{\pi RT_{\text{ave}}}}$
Kn < 0.01	$C_m = \frac{\varepsilon}{\tau\delta}\frac{PD_v}{P_a}\frac{M_w}{RT_{\text{ave}}}$
0.01 < Kn < 1	$C_{K+m} = \left(\frac{3\delta\tau}{2r\varepsilon}\sqrt{\frac{\pi RT_{\text{ave}}}{8M_w}} + \frac{\tau\delta}{\varepsilon}\frac{P_a}{PD_v}\frac{RT_{\text{ave}}}{M_w}\right)^{-1}$

The total heat transfer through the membrane ($\dot{Q}_m$) includes the conduction heat transfer ($\dot{Q}_c$) and the latent heat of vaporization ($\dot{Q}_v$) [29]

$$\dot{Q}_m = \dot{Q}_c + \dot{Q}_v = \frac{k_m}{\delta}(T_{\text{fm}} - T_{\text{pm}}) + JH_v \tag{13}$$

where H_v = 1,753.5T + 2,024.3 × 10^3 is the enthalpy of vaporization [20], $k_m = \left(\frac{\varepsilon}{k_g} + \frac{1-\varepsilon}{k_s}\right)^{-1}$ is the thermal conductivity of the membrane which is a function of the membrane porosity, the thermal conductivity of vapor (k_g) and the thermal conductivity of the membrane material (k_s) [32]. In DCMD systems, it is reported that 60%–80% of the total heat is transferred by the vapor across the membrane [26,33].

Temperature polarization is a well-known phenomenon in the MD system. It happens as a result of the heat transfer at both sides of the membrane, as shown in Fig. 1. Temperature polarization is responsible for reducing the driving force in DCMD systems. Temperature polarization coefficient (TPC) measuring the intensity of temperature polarization is defined as the ratio of the temperature difference across the membrane to the difference of bulk temperature of the feed and the permeate solution at the local cross section

$$\text{TPC} = \left(\frac{T_{\text{fm}} - T_{\text{pm}}}{T_f - T_p}\right) \tag{14}$$

The concentration polarization is a common issue in most membrane desalination processes [34–37]. As the water vapor passes through the membrane, the solute accumulates on the membrane surface causing the concentration polarization. The ratio of the local concentration on the membrane surface over the inlet feed concentration defines the concentration polarization coefficient (CPC) as follows:

$$\text{CPC} = \left(\frac{c_{\text{fm}}}{c_f}\right) \tag{15}$$

At the exit, the specified pressure and the zero-gradient for the temperature and concentration field are imposed in each channel. The inlet boundary conditions are as follows:

$$u = U_{f,\text{ave}},\ v = 0,\ w = 0,\ T = T_{f,\text{in}},\ c = c_{f,\text{in}}$$

for the feed stream (16)

$$u = U_{p,\text{ave}},\ v = 0,\ w = 0,\ T = T_{p,\text{in}},\ c = 0$$

for the permeate stream (17)

The membrane is treated as a functional surface where the water flux couples with the local feed and permeate temperature and the feed concentration. With the suction rate calculated by $V_m = J/\rho$, the membrane boundary conditions imposed on the surface of the membrane are as follows:

$$u = 0,\ v = V_m,\ w = 0,\ k_c \frac{\partial T}{\partial y} = -\dot{Q}_m \text{ and } D\frac{\partial c}{\partial y} = V_m c$$

at the feed side (18)

$$u = 0,\ v = -V_m,\ w = 0,\ k_c \frac{\partial T}{\partial y} = -\dot{Q}_m \text{ and } \frac{\partial c}{\partial y} = 0$$

at the permeate side (19)

The boundary conditions imposed on the feed and the permeate channel walls are as follows:

$$u = 0,\ v = 0,\ w = 0,\ \frac{\partial T}{\partial y} = 0, \text{ and } \frac{\partial c}{\partial y} = 0 \quad (20)$$

3. Numerical model and validation

Two three-dimensional geometries are considered. (1) The empty module containing rectangular-shaped feed and permeate flow channels separated by an active PTFE flat sheet membrane with the dimensions of each channel 50 h in length and 5 h in width where h is the height of the channel. (2) The module containing the net-type spacers in the feed and permeate channel with dimensions shown in Fig. 2. The spacers are placed in the middle of both channels 10 h away from the inlet and exit. The spacer's strand diameter is 0.5 h, and the angle between the strand and the horizontal direction is 45°. A total of eight cells are considered in the domain with a 5 h spacing between successive cells. The flow is laminar for each stream in the empty module, and the flow is turbulent for each stream in the module containing spacers. Fluent 17.1 was utilized to conduct simulations in three-dimensional DCMD module. The geometry of the module was created using SolidWorks and imported to the Ansys meshing tool for discretization. The membrane is treated as a functional surface where the suction rate, local temperature and concentration are coupled. The boundary conditions imposed at the surface of the membrane were executed using a user-defined function (UDF). The variation of the membrane permeability and the viscosity was also executed using a UDF. The density, specific heat and thermal conductivity of the feed and permeate solution were assumed constant [13]. The solute diffusion coefficient was considered constant [20]. The SIMPLE algorithm was used for the pressure-velocity coupling. The second order upwind algorithm was used for momentum, energy and user-defined scalar (solute transport). Reynolds number for flows in each channel, $\text{Re} = \frac{U_{\text{ave}}\rho h_d}{\mu}$, is defined based on the averaged flow velocity U_{ave} at the inlet and the channel hydraulic diameter h_d for each stream. Here ρ is the density and μ is the dynamic viscosity of each streaming fluids. In the permeate channel, the inlet temperature and Re are fixed at 20°C and 330 for all simulations.

A structured mesh is used for the empty channel geometry, and an unstructured mesh is used for the channel containing net-type spacers to discretize the domain. For both structured and unstructured meshes, an inflation layer is employed near the membrane surface on both sides of the channel to resolve velocity, temperature and concentration field inside the boundary layer. It was previously shown that a first layer thickness of 5 μm is resonable for capturing the concentration polarization [38]. The present simulations reveal that ±3 μm variations in the first layer thickness had

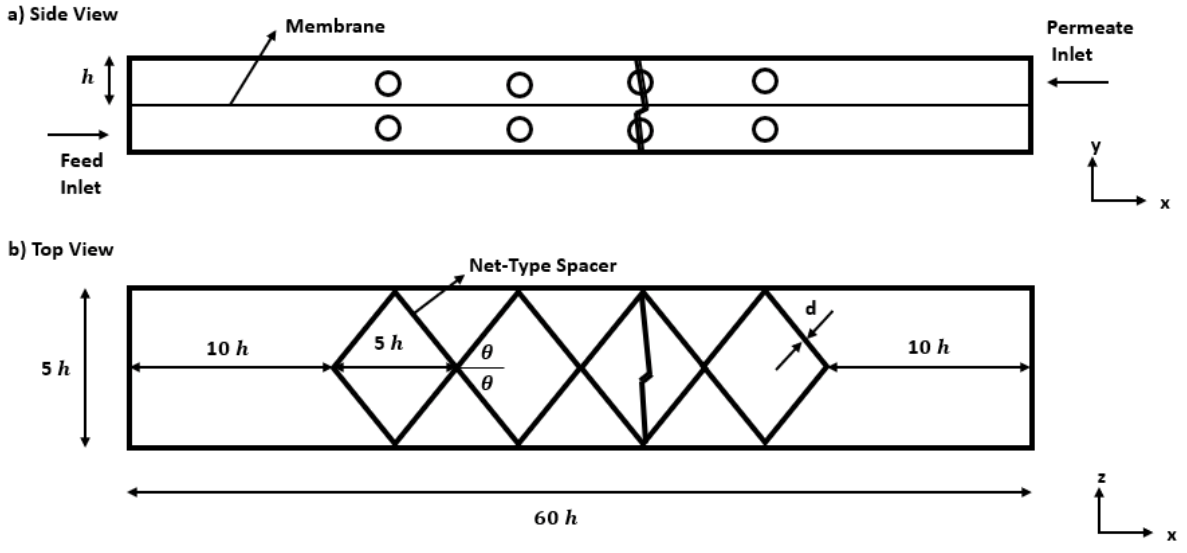

Fig. 2. Schematics of the module containing net-type spacers and dimensions of the geometry.

negligible influence on the prediction of the membrane performance. The mesh density of N1 = 1 million elements, N2 = 1.6 million elements, N3 = 3.2 million elements, and N4 = 6.4 million elements is selected to conduct the mesh independence test in the empty module for Re = 1,500 in the feed and Re = 330 in the permeate channel. Fig. 3a shows the normalized stream-wise velocity at x/h = 25 and z/h = 2.5. The velocity profiles obtained by the mesh density of N1, N2, N3, and N4 are nearly the same. Figs. 3b and c show the normalized concentration and temperature along the membrane surface at z/h = 2.5 from the inlet to the outlet. The temperature profiles at each side of the membrane predicted using N1, N2, N3, N4 are nearly identical. The concentration profiles at the feed side obtained by N1 and N2 display slight deviations while the concentration profiles obtained using N3 and N4 are nearly the same. It is concluded from the mesh optimization study that a mesh density of 3.2 million ensures spatial convergence for laminar flow simulation in the empty module. The spatial convergence of turbulent model simulations will be discussed below along with the validation study.

The mathematical model is validated using the experimental work by Termpiyakul et al. [39] conducted in DCMD membrane systems. In the experiment, the operational parameters used were: the concentrated feed solution 35 g kg^{-1}, the inlet feed temperature 60°C, the inlet permeate temperature 20°C, Re = 8,808 for the permeate channel flow and 9,900 ≤ Re ≤ 19,800 for the feed channel flow. These flow rates in each channel correspond to turbulent channel flows, so the validation test in the DCMD module was conducted using the k–ω shear stress transport model. The membrane properties for the validation study are taken from the experiments: the permeability of the PVDF membrane 6.67 × 10^{-7} kg m^{-2} s^{-1} Pa^{-1}, the thermal conductivity 0.041 W m^{-1} K^{-1}, and the thickness 126 μm. The permeate flux predicted agrees well with that measured for various values of the feed channel Re, as listed in Table 2. It is demonstrated that the mathematical models characterizing

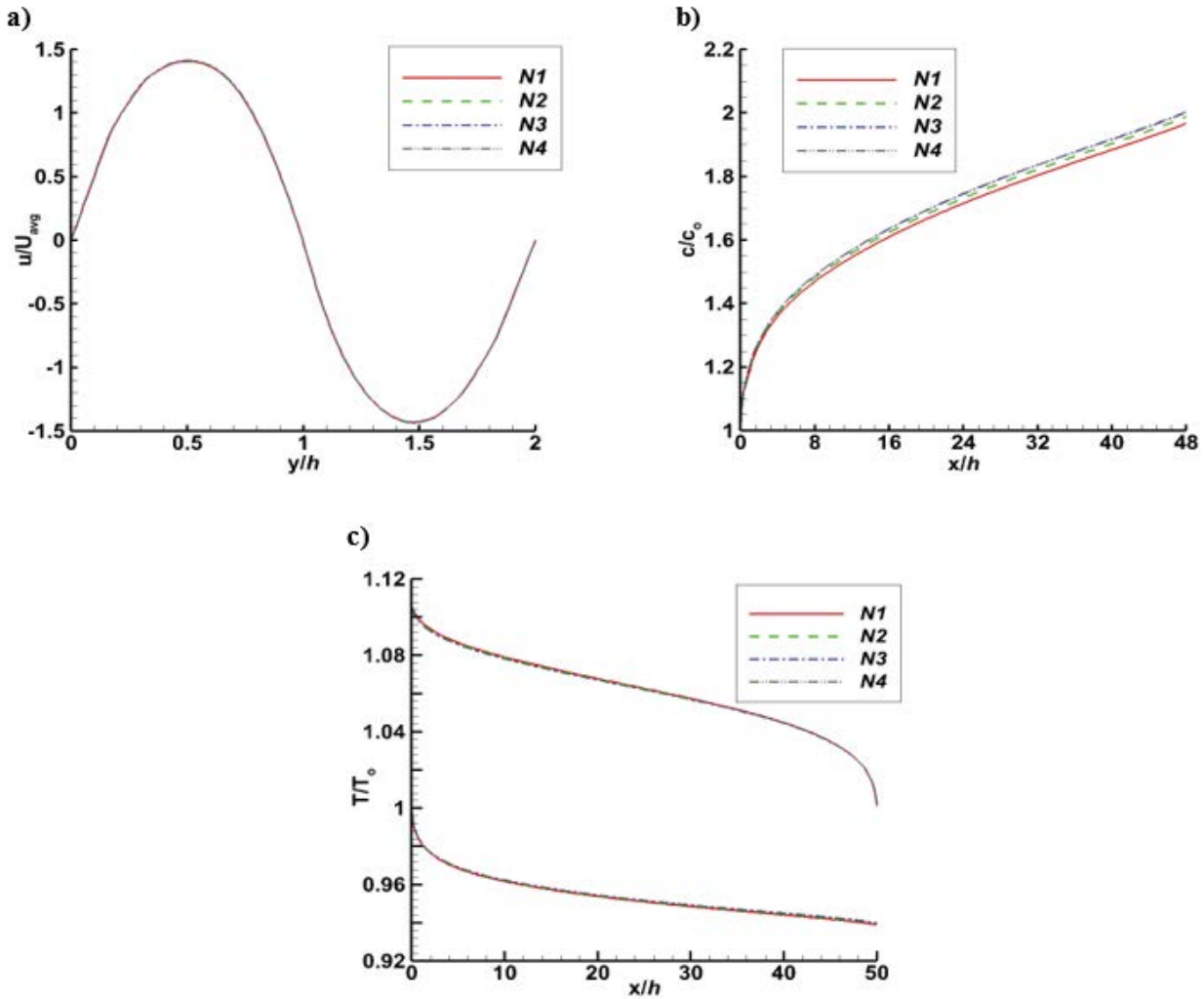

Fig. 3. Profiles of (a) the stream-wise component of the velocity at z/h = 2.5 and x/h = 25, (b) the normalized concentration over the surface of the membrane in the feed side at z/h = 2.5 and (c) the normalized temperature over the surface of the membrane in the feed and permeate side at z/h = 2.5. The profiles are acquired using the mesh density of N1 = 1 million, N2 = 1.6 million, N3 = 3.2 million and N4 = 6.4 million elements.

Table 2
Permeation flux predicted and measured for various values of the feed channel Re

Re	Permeation flux (kg m^{-2} h^{-1})		
	Experiment	Simulation	Deviation %
9,900	30.80	32.50	5.50
14,861	37.80	36.50	3.60
19,780	39.00	37.40	4.30

the transport phenomena in both channels and through the membrane are validated. The mesh density of 10.5 million elements with the maximum y+ value of about 0.3 is used in the validation study. The predictions for the validation simulations obtained using 6 million and 10.5 million mesh are nearly the same. Turbulent flow simulations conducted in the module containing spacers employ the mesh with 30 million elements (a sample of the mesh is shown in Fig. 4), having the similar resolution near the membrane surface (y+ is less than 0.4) as the mesh used in the validation study to ensure that the boundary layers are accurately resolved. The velocity, concentration and temperature field simulated with the mesh density of 30 and 40 million are very similar (not presented here).

4. Results and discussion

4.1. Parametric study – empty module

The results of the parametric study evaluating the effects of the membrane properties and the system operating parameters on the separation system performance are presented. The permeability has a profound influence on the MD system performance. Membranes of the type hydrophobic polyvinylidene fluoride (PVDF) suffers from low values of permeability (ranging from 3.00×10^{-7} to 7.00×10^{-7} kg m^{-2} Pa^{-1} s^{-1}). Recently, researchers developed polytetrafluoroethylene (PTFE) membranes which posses higher permeability than PVDF membranes. PTFE membranes have a permeability in the range of (6.00×10^{-7} to 2.40×10^{-6} kg m^{-2} Pa^{-1} s^{-1}) [29]. The membrane thickness, porosity, and pore size are other properties that could have a strong influence on the system performance. For typical MD membranes, the thickness ranges from 30 to 180 μm, the porosity ranges from 0.6 to 0.88, and the average pore size ranges from 0.2 to 1 μm. Table 3 shows a list of the properties of the active layer membrane used in the parametric study. The selected range of parameters is motivated by the existing commercial membranes [27].

Fig. 5 shows the average water flux as a function of the thickness for values of the porosity 0.6, 0.7 and 0.8 and the pore size 0.2, 0.45 and 1 μm. For the values of the pore size considered, the Knudsen number is calculated to be in the range of 0.01 and 1, as listed in Table 4. The permeate

Table 3
Membrane parameters used in the simulations

Parameter	Values
Membrane thickness, δ	100, 130 and 170 (μm)
Membrane porosity, ε	0.6, 0.7 and 0.8 (–)
Membrane pore size, d_p	0.20, 0.45 and 1.0 (μm)

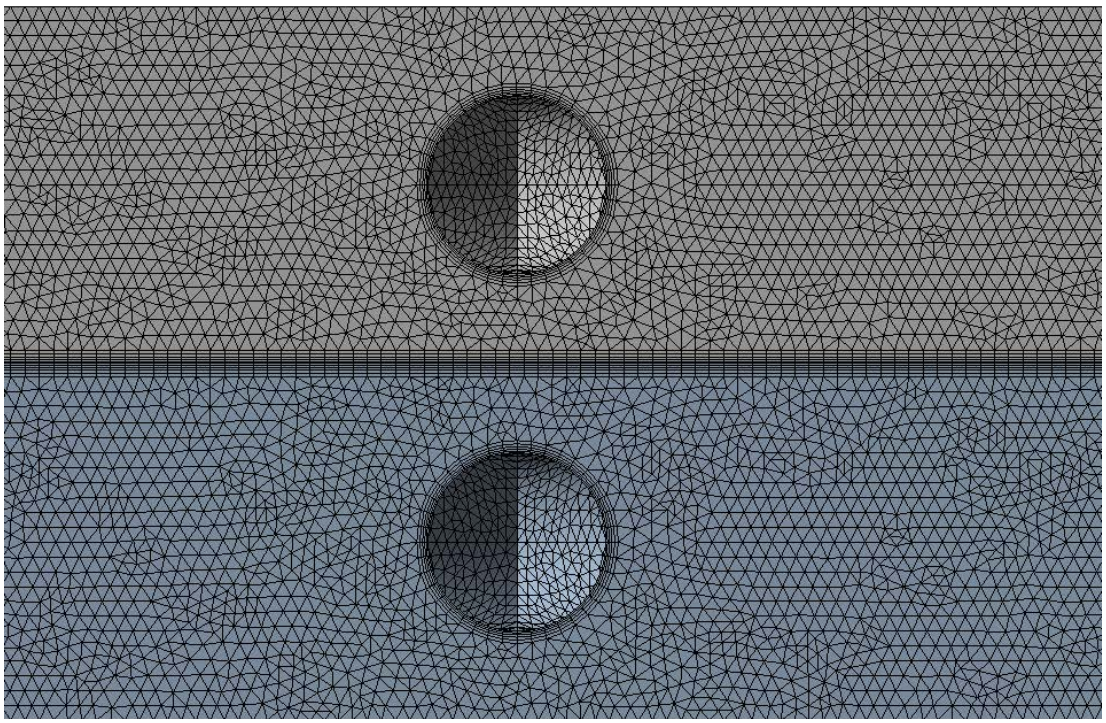

Fig. 4. A sample of the unstructured mesh for the geometry with net-type spacers.

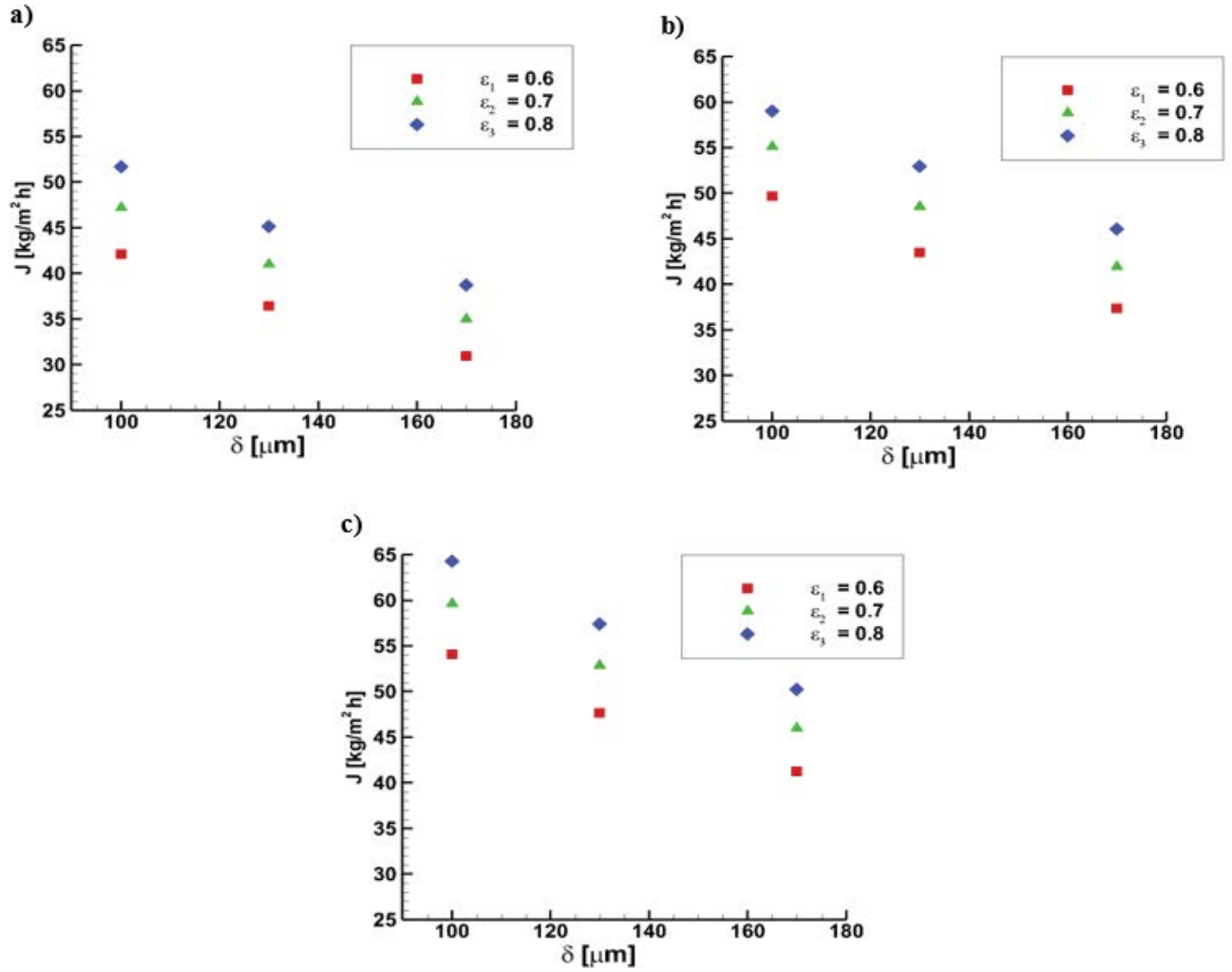

Fig. 5. Area-averaged water flux for various values of the membrane thickness and the porosity of (a) pore size = 0.20 μm, (b) pore size = 0.45 μm and (c) pore size = 1 μm.

Table 4
Knudsen number values for the selected pore sizes

Pore Size (μm)	Knudsen number [–]
0.20	0.78
0.45	0.35
1.00	0.16

flux through the membrane should be determined from the Knudsen and molecular diffusion combined, and the permeability coefficient is calculated using the relation presented in Table 1. For d_p = 0.2 μm, the highest water flux is attained with the membrane possessing the highest porosity and the lowest thickness while the lowest flux is attained with the membrane possessing the lowest porosity and the highest thickness, as depicted in Fig. 5a. For the same membrane thickness, the permeate flux increases as the porosity increases, and for the same porosity, the water flux decreases as the thickness increases. The similar trend is observed for d_p = 0.45 and 1 μm, as depicted in Figs. 5b and c. For d_p = 0.45 μm, the water flux level is slightly elevated for all values of the thickness and the porosity as compared with that for d_p = 0.2 μm, even though, the pore size is increased by 125%. Similarly, with an 122% increase in the pore size between d_p = 1 μm and d_p = 0.45 μm, the minuscule increase is observed in the permeated water flux (Figs. 5b and c). The weak dependence of the flux on the pore size can be attributed to the fact that the membrane considered here permit flux by the Knudsen and the molecular diffusion. The resistance to the Knudsen diffusion is inversely proportional to the pore radius while the resistance to the molecular diffusion is independent of the pore size. The total resistance of the membrane to the mass diffusion is determined using the parallel circuit of the Knudsen and the molecular diffusion resistors, as presented in Table 1. Hence, the change of the pore radius does not pose a strong influence on the total membrane resistance. On the contrary, the effect of the pore size on the permeated flux is very strong for the VMD process since the total resistance of VMD membrane is determined by the Knudsen and viscous

diffusion resistors connected in parallel and both resistances are a strong function of the pore size. On the other hand, the membrane thickness has a stronger influence on the water flux in the DCMD module compared with that in the VMD module. Such an in-depth comparison between the DCMD and VMD module was made possible from the results of the parametric study conducted by Usta et al. [40] for the VMD process. The increase in the pore size will make the MD membranes susceptible to wetting as the liquid entry pressure decreases with the increased pore size. The pore size $d_p \leq 0.5$ μm is recommended for the DCMD module [41–43].

Fig. 6 shows the average temperature polarization coefficient in DCMD systems. Ideally, the TPC should have the value of unity when there is no temperature polarization – the temperature over the membrane surface at each side would be equal to the temperature of the bulk stream in each channel. However, since there is heat removed (vaporization) from the feed solution and gained (condensation) by the cold stream over the surface of the membrane the thermal boundary layer forms at each side and the temperature polarization occurs naturally as a result. The temperature polarization has an undesirable influence on MD performance, and it needs to be mitigated. Moreover, unlike other membrane distillation systems, there could be significant conductive heat losses across the DCMD membranes which also hinder the system performance. Fig. 6 shows the TPC for various values of the pore size and membrane thickness and porosity. There is a direct relationship with the intensity of the temperature polarization and the level of permeate flux through the membrane – the intensity of temperature polarization increases as the water flux increases. As the water permeation increases, TPC becomes smaller, as shown in Figs. 5 and 6. The value of TPC being further away from the unity represents the occurrence of more intense temperature polarization in the module. The heat removed from the feed solution increases linearly with the increase in the permeate flux; causing a steeper temperature gradient across the thermal boundary layer attached to each side of the membrane. Fig. 6 shows that TPC varies from about 0.67 to nearly 0.43, indicating a serious level of temperature polarization occurs in the system.

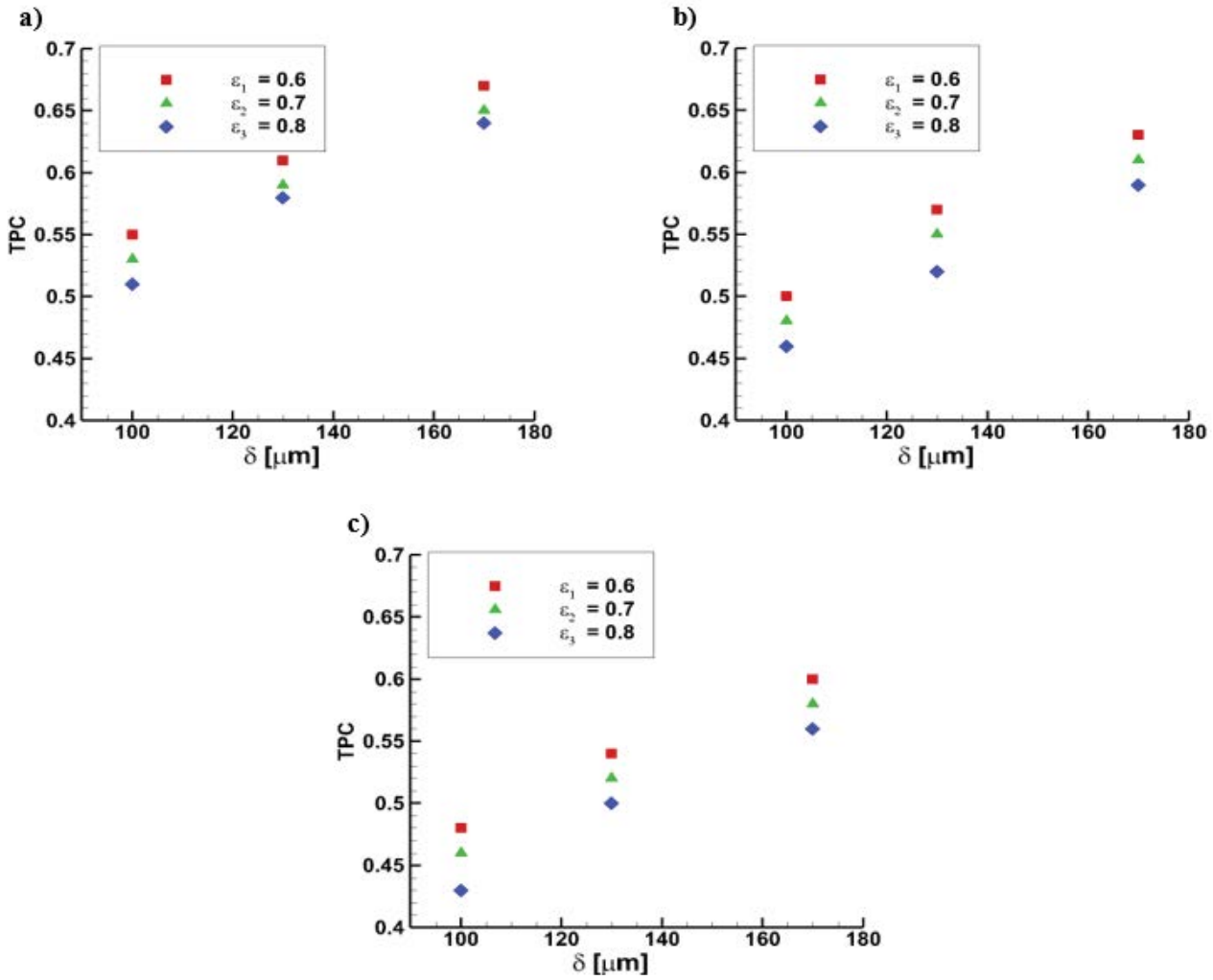

Fig. 6. Area-averaged temperature polarization coefficient for various values of the membrane thickness and the porosity of (a) pore size = 0.20 μm, (b) pore size = 0.45 μm and (c) pore size = 1 μm.

The concentration polarization is another critical factor determining system separation performance. Fig. 7 shows the average concentration polarization over the membrane surface in the feed channel. It is preferred for the CPC to be near unity. Similarly, the concentration polarization is inevitable as the water permeates from the feed channel to the permeate channel; the solute concentration near the membrane increases and the concentration boundary layer is formed. Similar to the temperature polarization, the concentration polarization is directly correlated with the magnitude of the water flux – the intensity of concentration polarization increases as the rate of permeated water is increased, as depicted in Figs. 5 and 7. Fig. 7 shows that the value of the CPC as high as about 1.7 and as low as about 1.25 is observed as the membrane properties are varied. The concentration polarization has an adverse effect over the membrane system as it reduces the water flux. It is also important to mention that the membrane fouling occurs for the continuous operation of membrane separation. The regions where fouling would occur are strongly correlated to the high concentration polarization regions over the membrane surface [35]. The remedies alleviating the concentration polarization should be considered in the design of these modules.

It was deduced that the membrane with thickness of 100 μm, pore size of 0.45 μm and porosity of $\varepsilon_3 = 0.80$ yield good flux performance. The effects of the operating parameters on the flux performance and the polarization are examined next. It was shown in the previous study [44] that the operating parameters of the permeate channel have a weak influence on the system performance. The permeate inlet temperature ranges between 5°C and 25°C in typical applications and the vapor pressure changes slightly for this range of temperature. In this work, the operating parameters controlling conditions in the feed channel are considered in the parametric study. The inlet temperature and Re in the permeate channel are fixed at 20°C and 330 while the inlet temperature and Re in the feed channel are varied. The inlet concentration of the feed solution is taken as 35 g kg^{-1}, which corresponds to the sea water desalination. Table 5 lists the range of the feed inlet temperature and the flow rate considered in the simulations.

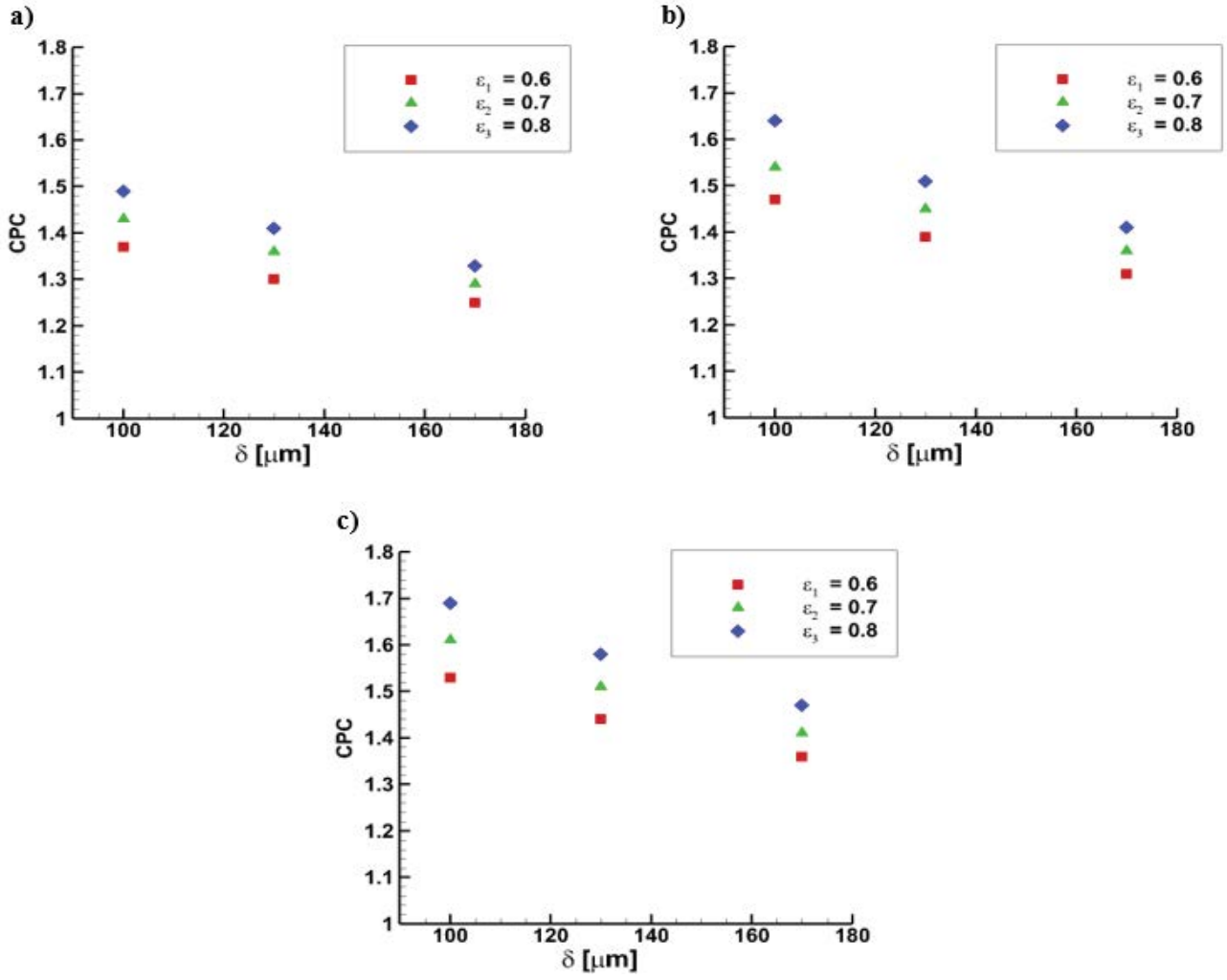

Fig. 7. Area-averaged concentration polarization coefficient for various values of the membrane thickness and the porosity of (a) pore size = 0.20 μm, (b) pore size = 0.45 μm and (c) pore size = 1 μm.

Table 5
Feed operating parameters used in the simulations

Fixed parameters	Re = 1,500				T = 80°C			
Variable parameters	T (°C)				Re			
	50	60	70	80	100	500	1,000	1,500

Fig. 8 shows the average water flux, the coefficients of the temperature and the concentration polarization as a function of the inlet feed temperature at Re = 1,500. The vapor pressure in the feed channel increases exponentially with increasing the feed temperature as predicted by the Antoine equations (Eq. (12)). The water flux increases from 18.5 kg m^{-2} h^{-1} at 50°C to 59.05 kg m^{-2} h^{-1} at 80°C, as shown in Fig. 8a. The effects of the local concentration at the membrane surface are included in the flux model employed in the present study even though most researchers ignore such effects [15]. Furthermore, the flux equation couples both feed and permeate temperatures along with the feed concentration to accurately predict the variation of the water flux along the membrane surface. The TPC reduces and CPC increases as the inlet feed temperature is increased, as depicted in Figs. 8b and c. The heat absorbed from the feed solution by vaporization and the heat released to the cold stream by condensation increase as the rate of water permeate increases. There is another reason for the decrease of TPC: the heat loss by the conduction through the membrane. The average concentration polarization can be estimated from the water flux information by using the exponential relation given as $\exp\left(\frac{J}{D\,\rho}\right)$ where D is the diffusivity and ρ is feed density. The fouling induced by the concentration polarization would add extra resistance to the transfer of water vapor through the membrane and will reduce the life span of the membrane [34,35,37]. It is deduced from results that the use of mixing promoters is desired especially during operations with the higher inlet feed temperature due to the occurrence of more intense concentration and temperature polarization at these conditions. Mixing feed solution will mitigate both concentration and temperature polarization.

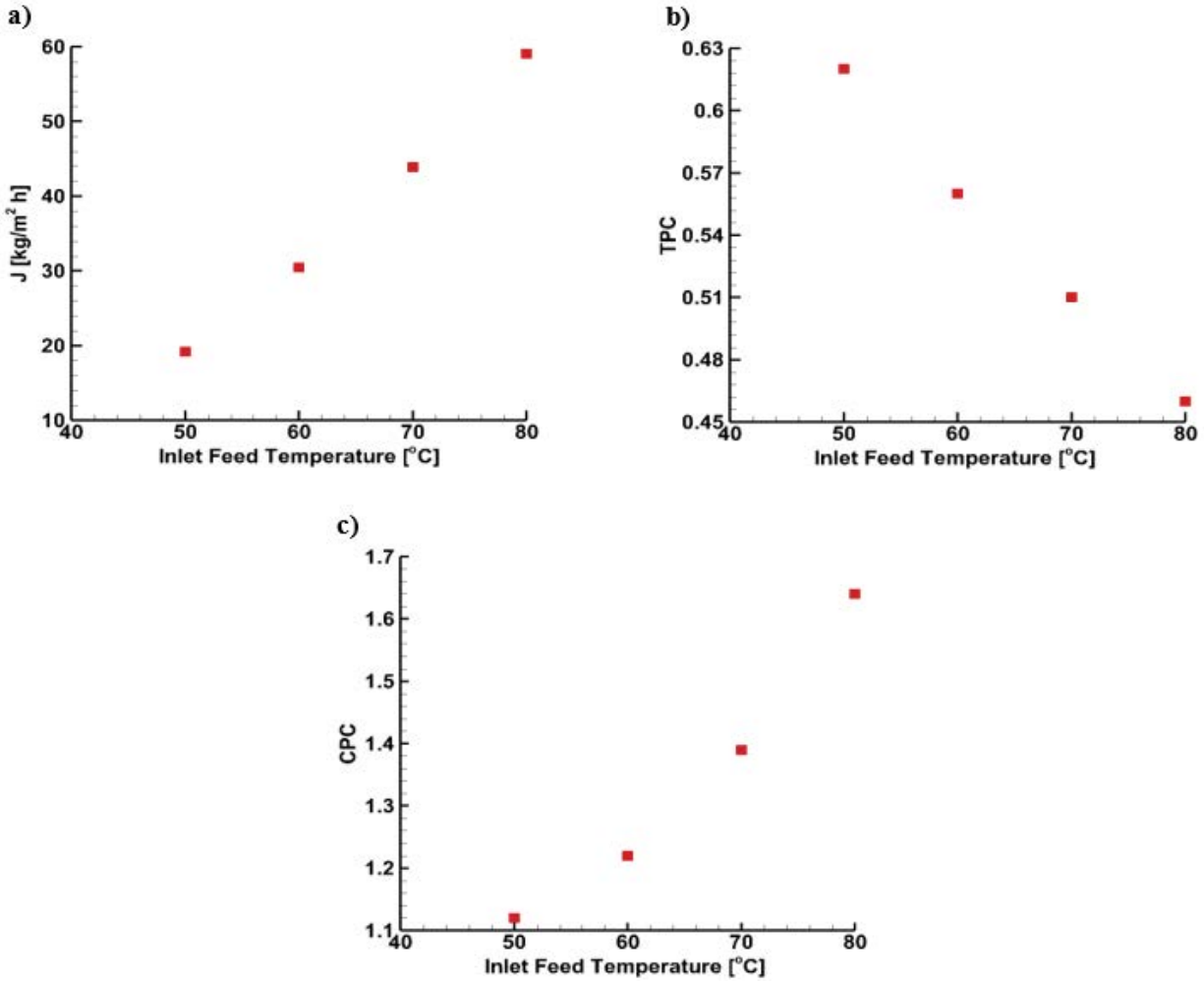

Fig. 8. Area-averaged (a) water flux, (b) temperature polarization coefficient, (c) concentration polarization coefficient as a function of the inlet feed temperature.

Fig. 9 shows the average water flux, the coefficients of the temperature and the concentration as a function of the flow rate at the inlet feed temperature of 80°C. The water flux increases as the feed flow rate increases, as shown in Fig. 9a. The rate of water permeation is increased from nearly 32.31 kg m^{-2} h^{-1} at Re = 100 to about 59.05 kg m^{-2} h^{-1} at Re = 1,500. The increase with Re is abrupt at lower flow rates but becomes gentler at higher flow rates; a nearly asymptotic value is reached as the flow rate is increased. The improvement in the water flux is limited by the nature of the laminar flow. If the flow regime becomes turbulent, the improvement in the water flux could be amplified since the turbulent flows induce more mixing in both channels.

The intensity of the temperature polarization improves slightly as the flow rate is increased – TPC is increased from about 0.39 to about 0.46 as Re is increased from 100 to 1,500, as shown in Fig. 9b. At Re = 100, the thermal boundary layer is thick at the feed side; causing a drop in the value of the TPC. The thermal boundary layer becomes thinner as the flow rate is increased and the value of TPC increases. Within the laminar flow regime, TPC tends to the asymptotic value as Re is increased. The effect of the flow rate on the concentration polarization is stronger (Fig. 9c). The enhanced momentum mixing in the feed channel with increasing flow rate aids in reducing the intensity of concentration polarization. At Re = 100 CPC is about 2.4, and it diminishes to about 1.65 for Re = 1,500. In DCMD modules, the influence of the concentration polarization on the membrane flux performance is not overwhelming as in other separation modules such as reverse osmosis and forward osmosis. Boubakri et al. [45] conducted experiments to compare the water flux with the pure water in the feed channel and with the highly concentrated feed water. The difference between the water flux obtained with a feed concentration of 40 g kg^{-1} and with the pure water was 1.5%. This reduction does not account for the effect of fouling over the membrane. Fouling will reduce the water flux and cause membrane degradation over a longer period of operation [46]. Hence, it is still vital to mitigate concentration polarization to reduce the chance of fouling over the membrane surface [2]. A similar finding concerning the effect of feed concentration on the water flux output was reported by Al-Mutaz et al. [47].

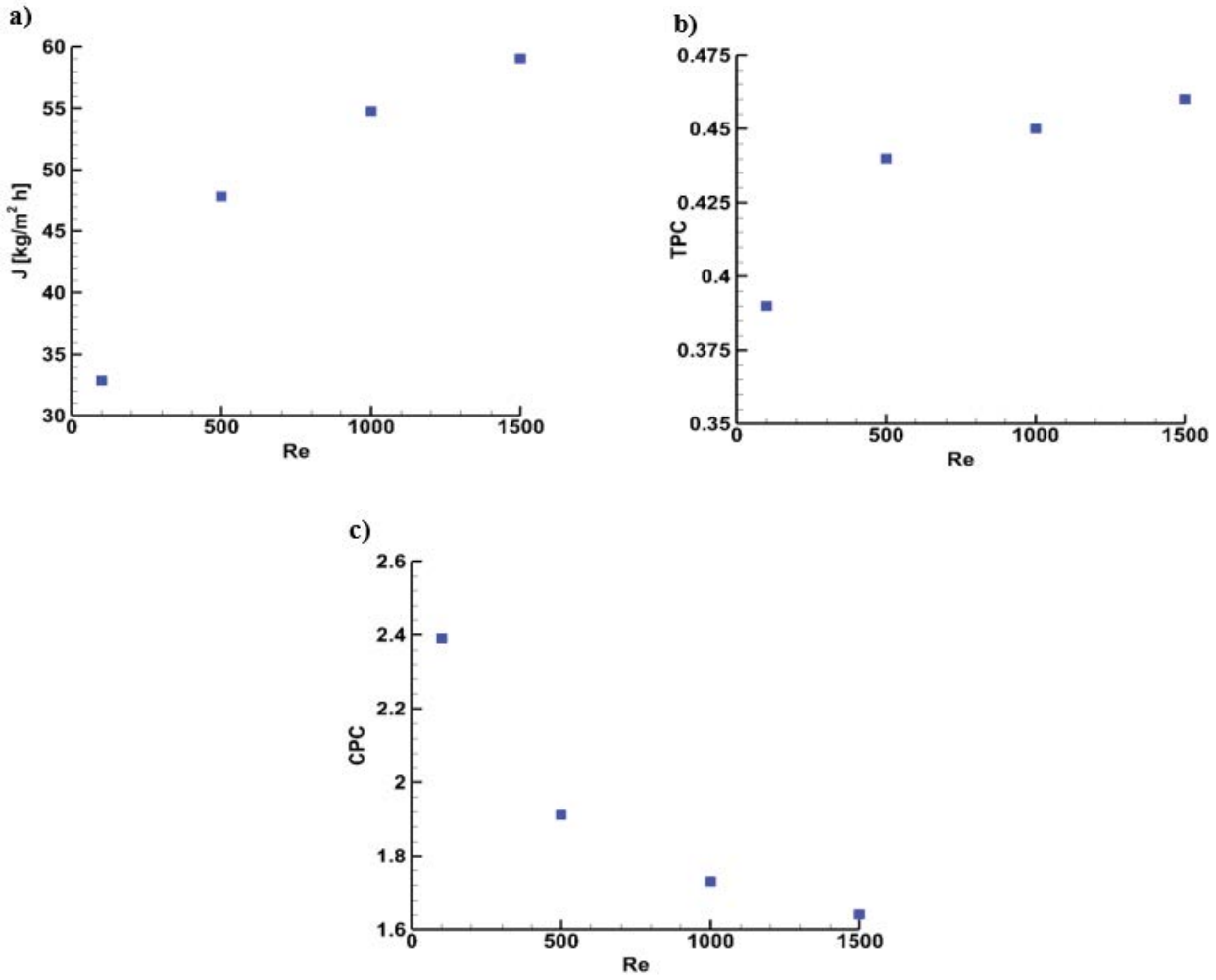

Fig. 9. Area-averaged (a) water flux, (b) temperature polarization coefficient and (c) concentration polarization coefficient as a function of the feed flow rate.

4.2. Mitigation of polarization – module containing spacers

The results obtained from simulations in the module containing the net-type of spacers at the feed Re = 100; 500; 1,000 and 1,500 and the permeate Re = 330 for the inlet feed and permeate temperature of 80°C and 20°C, respectively, are presented next. The membrane properties selected are the thickness 100 μm, the pore size d_p = 0.45 μm, and the porosity ε_3 = 0.80. The objective here is to demonstrate the efficacy of using spacers in enhancing the membrane flux performance and alleviating polarizations.

Fig. 10 shows contours of the stream-wise velocity in the feed channel, the suction rate, wall shear stress, temperature and concentration along the membrane surface at the feed side for 23 ≤ x/h ≤ 47. Fig. 10a shows the normalized stream-wise velocity at the plane y/h = 0.75 between the membrane surface and the spacers. Repeated patterns of high and low-speed flow regions in the feed channel following the cells of spacers are observed. The water flux was normalized with the pure water permeability and the vapor pressure difference determined at the inlet temperature of the feed and the permeate solution. Patterns of high and low water flux regions are observed over the membrane surface succeeding the spacer cells. The high-water flux regions correlate with the high-speed regions, but the correlation is not as strong since the water flux is influenced by the flow and temperature field of each stream. There is also a correlation between the wall shear stress and the water flux patterns. The low shear stress regions seen behind the intersection of strands correspond to low values of water flux, as depicted in Figs. 10b and c. The maximum (0.7) and minimum (0.4) value of the normalized water flux obtained in the module correspond to 101.54 and 58.03 kg m^{-2} h^{-1}. Figs. 10d and e show the concentration and temperature contours over the membrane surface. The correlation between the high wall shear stress regions and regions with the low concentration polarization is not as obvious as in the reverse osmosis separation modules [35,37]. It is clear that the temperature polarization is more intense in regions with high vapor permeation, as expected since the temperature polarization is induced by the vaporization.

Fig. 11 shows contours of the stream-wise velocity, the wall shear stress and the temperature over the membrane surface at the permeate side for 15 ≤ x/h ≤ 35. Repeated patterns of the flow and temperature field follow the cells of spacers. The high wall shear stress regions are observed above the spacers while lower shear stress regions are seen inside each cell. The correlation between the high-temperature regions and low wall shear stress regions is stronger in the permeate channel compared with that in the feed channel. The temperature polarization of the module is determined by the membrane surface temperature and the bulk temperature of each flow. The more complex relationship between polarization and the flow field in the DCMD module compared with other membrane separation modules.

The influence of the net-type of spacers on the membrane performance by comparing the area averaged values of the permeate flux, TPC and CPC obtained for the empty module and the module containing spacers at various values of the feed Re is quantified. The value of CPC decreases while the value of TPC increases in the module containing spacers at all flow rates; meaning the concentration and temperature polarization are mitigated by the spacers. The alleviation of temperature and concentration polarization is lower at the lower flow rate, and it is capped as flow rate is increased – the level of polarization reduction at Re of 1,000 and 1,500 is nearly the same. The permeation flux is also greater in the module containing spacers at all flow rates, but the increase of flux is minute at Re = 100, as listed in Table 6. The flux is increased by 40.7% at Re = 500 and up to 51.1% at Re = 1,500; revealing that the spacers are more effective at higher flow rates.

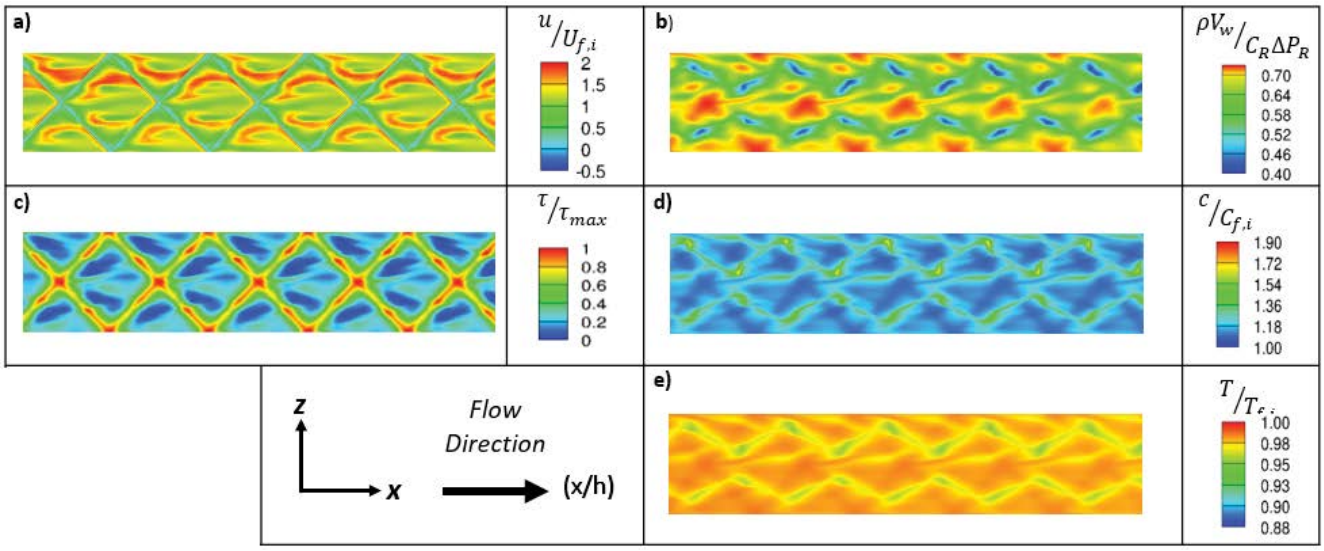

Fig. 10. Contours (a) the normalized stream-wise velocity at y/h = 0.75, (b) the normalized suction velocity, (c) the normalized wall shear stress, (d) the concentration and (e) the temperature over the surface of the membrane at the feed side. Images are rendered at 23 ≤ x/h ≤ 47 for Re = 1,500.

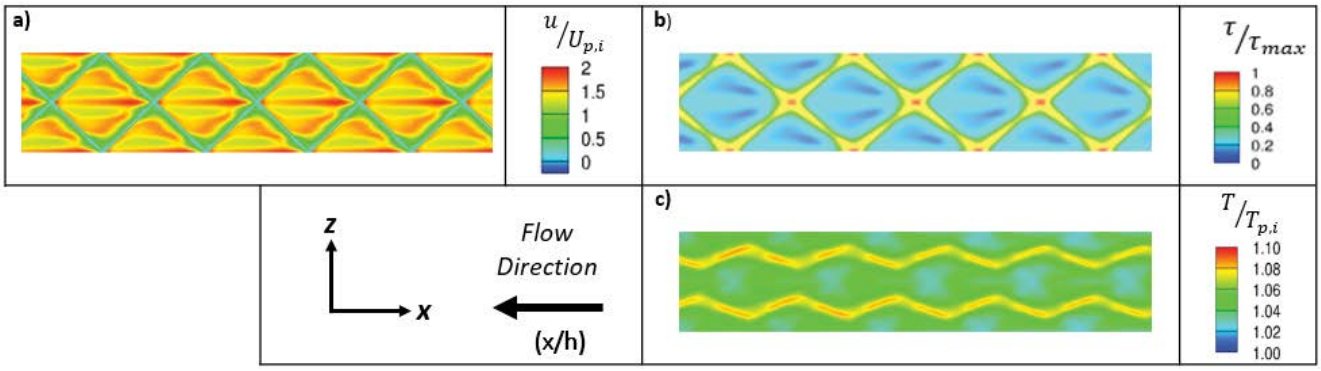

Fig. 11. Contours (a) the normalized stream-wise velocity at y/h = 1.75, (b) the normalized wall shear stress and (c) the temperature over the surface of the membrane at the permeate side. Images are rendered at $15 \le x/h \le 35$ for Re = 330.

Table 6
Area-averaged concentration and temperature polarization coefficients and the water flux in the module with and without spacers at various values of feed stream Re

Re	100			500			1,000			1,500		
	CPC	TPC	J	CPC	TPC	J	CPC	TPC	J	CPC	TPC	J
Empty	2.39	0.39	32.31	1.91	0.44	47.81	1.73	0.45	54.76	1.64	0.46	59.05
Spacers	1.90	0.44	34.49	1.36	0.56	67.29	1.29	0.59	81.56	1.24	0.60	89.22
% Change	20.5	12.8	6.7	28.7	27	40.7	25.4	31	48.9	32.2	30.4	51.1

Table 7
Energy balance and pumping power for the DCMD system

	$\dot{Q}_f$ (kW m^{-2})	$\dot{Q}_c$ (kW m^{-2})	$\dot{Q}_v$ (kW m^{-2})	$\dot{Q}_c/(\dot{Q}_c+\dot{Q}_v)$	$\dot{Q}/\dot{Q}_f$
Empty	50.4	7.88	42.52	15.6%	0.0022%
Spacer	74.6	10.26	64.33	13.76%	0.013%

The main energy input to any MD desalination system is in the form of heating and cooling. In DCMD systems, the feed solution is typically heated to a temperature between 50°C and 80°C while the permeate fluid is cooled to a temperature between 20°C and 25°C. Pumping power is considered as auxiliary power, and it is usually ignored in the performance consideration. The total thermal power input for the feed solution is follows:

$$\dot{Q}_f = \dot{Q}_{\text{in}} - \dot{Q}_{\text{out}} = \dot{m} c_p T_{\text{in}} - \rho c_p \int T\, u\, dA = \dot{Q}_c + \dot{Q}_v \tag{21}$$

where $\dot{m}$ is the mass flow rate of the feed water, c_p is the specific heat of water and T_{in} is the inlet feed temperature, ρ is the density of the water in the feed channel and u is the stream-wise component of the velocity of the feed solution at the exit. The total thermal power input of the feed channel is transferred through the membrane by vaporization and the conduction and it will be equivalent to the thermal power input of the permeate channel to cool the permeate solution since the module is assumed to be well insulated. The heat consumed by the evaporation is beneficial and it will increase only when the rate of water permeation increases. The pumping power requirement of the feed flow is calculated $\dot{P} = \Delta P\, A\, U_{f,\text{ave}}$, where ΔP is the pressure drop and A is the cross-sectional area of the feed channel.

Table 7 shows the thermal power input of the feed solution in the module without and with the spacers at Re = 1,500. The conductive power loss in the module without and with spacers is 15.6% and 13.76% of the total thermal power input, respectively, revealing that the conductive losses are smaller compared with the heat transferred by the phase change in each module. The heat transfer by the vaporization increases in the module containing spacers since the rate of vapor permeation increases. The conductive heat transfer across the membrane is also increased by the presence of spacers due to the mixing effects. The pumping power is only a small fraction of the required heat input to the system in each module. Luo and Lior [48] have reported that the pumping power is around 0.5% of the heat input to the DCMD module. The results reveal that the pumping power for the empty module and the module with spacers was 0.0022% and 0.013%, respectively. Results predicted by the energy analysis are consistent with results reported in the literature by the experimental studies, thus further validates the mathematical model and numerical methods.

5. Conclusion

Computational fluid dynamic simulations were conducted to study the flux performance, temperature and concentration polarization characteristics of the DCMD module performing the seawater desalination process. A parametric study was performed to access the influence of the membrane properties and operating parameters on the system performance within an empty module utilizing laminar flow simulations. The *k*-ω SST turbulence model was employed to characterize the velocity, temperature and concentration field, the membrane flux and polarization characteristics in the module containing net-type spacers. The mathematical model accounts for the variation of the membrane permeability as a function of both feed and permeate temperature. The values of the vapor pressure in both channels were determined using the Antoine equation with the added term accounting for the effect of the solute concentration. The mathematical model was validated using the existing experimental results. The permeate flux increases as the thickness is decreased and the porosity and the pore size are increased. The pore size has a lesser influence compared with the membrane thickness and porosity. The water flux and the intensity of temperature and concentration polarization are much greater at the higher inlet temperature of the feed solution. The increased feed flow rate improves the temperature and concentration polarization, but the polarization mitigation is limited when flow regime in channels is laminar. The overall module separation performance is improved in the module containing net-type spacers at all flow rates. It is demonstrated that the presence of spacers in both channels enhances the membrane flux performance more than 50% and mitigate temperature and concentration polarization up to 30% at higher flow rates. Although the pressure drop increased with the presence of spacers, the percentage of pumping power to the heat input to the system is still negligible for all cases considered. It is also demonstrated that the conductive losses across the membrane are less than 16% of the total thermal power input of the module. It is recommended that a more detailed parametric study is to be conducted on the design of the spacer geometry for better system performance.

Nomenclature

c	—	Solute mass fraction, $kg_{solute}\ kg^{-1}_{water}$
c_p	—	Specific heat of the water, kJ kg^{-1} K^{-1}
d_p	—	Membrane pore diameter, m
h_d	—	Channel hydraulic diameter, m
k_w	—	Thermal conductivity of water, W m^{-1} K^{-1}
k_g	—	Thermal conductivity of the gas, W m^{-1} K^{-1}
k_m	—	Thermal conductivity of the membrane, W m^{-1} K^{-1}
k_s	—	Thermal conductivity of the solid, W m^{-1} K^{-1}
$\dot{m}$	—	Mass flow rate of the feed water, kg s^{-1}
r	—	Membrane pore radius, m
p	—	Pressure, Pa
A	—	Cross-sectional area of the feed channel, m^2
C	—	Membrane permeability, kg $m^{-2}Pa^{-1}$ s^{-1}
D	—	Solute diffusion coefficient, m^2 s^{-1}
D_v	—	Diffusion coefficient of vapor, m^2 s^{-1}
H_v	—	Enthalpy of water vaporization, J kg^{-1}
J	—	Permeate flux, kg m^{-2} s^{-1}
K_B	—	Boltzmann constant, m^2 kg s^{-2} K^{-1}
M_w	—	Molecular weight of water, kg mol^{-1}
$\bar{P}$	—	Average pressure within the membrane pores, Pa
P_a	—	Pressure inside the membrane pore, Pa
P_v	—	Vapor pressure, Pa
$\dot{P}$	—	Pumping power, W
$\dot{Q}_m$	—	Total heat transfer through the membrane, W m^{-2}
$\dot{Q}_f$	—	Total thermal power input for the feed solution, W m^{-2}
$\dot{Q}_c$	—	Conduction heat transfer, W m^{-2}
$\dot{Q}_v$	—	Heat of vaporization, W m^{-2}
R	—	Universal gas constant, m^2 kg s^{-2} K^{-1} mol^{-1}
Re	—	Reynolds number
T	—	Temperature, K
$\overrightarrow{U}$	—	Velocity vector, m s^{-1}
V_m	—	Suction rate, m s^{-1}

Greek Letters

ρ	—	Density, kg m^{-3}
μ	—	Viscosity, Pa s
λ	—	Mean free path
σ	—	Collision diameter of the water, m
δ	—	Membrane thickness, m
τ	—	Membrane tortuosity
ε	—	Membrane porosity

Acknowledgments

This work used Extreme Science and Engineering Discovery Environment (XSEDE) for running CFD simulations, which is supported by National Science Foundation grant number TG-CT170051. This work used the Bridges system at the Pittsburgh Supercomputing Center (PSC).

References

[1] I.C. Karagiannis, P.G. Soldatos, Water desalination cost literature: review and assessment, Desalination, 223 (2008) 448–456.
[2] K.P. Lee, T.C. Arnot, D. Mattia, A review of reverse osmosis membrane materials for desalination — development to date and future potential, J. Membr. Sci., 370 (2010) 1–22.
[3] B.L. Pangarkar, S.K. Deshmukh, V.S. Sapkal, R.S. Sapkal, Review of membrane distillation process for water purification, Desal. Wat. Treat., 57 (2016) 2959–2981.
[4] K. Zhani, K. Zarzoum, H. Ben Bacha, J. Koschikowski, D. Pfeifle, Autonomous solar powered membrane distillation systems: state of the art, Desal. Wat. Treat., 57 (2016) 23038–23051.
[5] J. Zhang, N. Dow, M. Duke, E. Ostarcevic, J.-D. Li, S. Gray, Identification of material and physical features of membrane distillation membranes for high performance desalination, J. Membr. Sci., 349 (2010) 295–303.
[6] A.M. Alklaibi, N. Lior, Membrane-distillation desalination: status and potential, Desalination, 171 (2005) 111–131.
[7] M.S. El-Bourawi, Z. Ding, R. Ma, M. Khayet, A framework for better understanding membrane distillation separation process, J. Membr. Sci., 285 (2006) 4–29.
[8] S. Adnan, M. Hoang, H. Wang, Z. Xie, Commercial PTFE membranes for membrane distillation application: effect of microstructure and support material, Desalination, 284 (2012) 297–308.
[9] R. Bouchrit, A. Boubakri, A. Hafiane, S.A.-T. Bouguecha, Direct contact membrane distillation: capability to treat hyper-saline solution, Desalination, 376 (2015) 117–129.

[10] L. Francis, N. Ghaffour, A.S. Alsaadi, S.P. Nunes, G.L. Amy, Performance evaluation of the DCMD desalination process under bench scale and large scale module operating conditions, J. Membr. Sci., 455 (2014) 103–112.
[11] H.J. Hwang, K. He, S. Gray, J. Zhang, I.S. Moon, Direct contact membrane distillation (DCMD): experimental study on the commercial PTFE membrane and modeling, J. Membr. Sci., 371 (2011) 90–98.
[12] J.-M. Li, Z.-K. Xu, Z.-M. Liu, W.-F. Yuan, H. Xiang, S.-Y. Wang, Y.-Y. Xu, Microporous polypropylene and polyethylene hollow fiber membranes. Part 3. Experimental studies on membrane distillation for desalination, Desalination, 155 (2003) 153–156.
[13] H. Yu, X. Yang, R. Wang, A.G. Fane, Numerical simulation of heat and mass transfer in direct membrane distillation in a hollow fiber module with laminar flow, J. Membr. Sci., 384 (2011) 107–116.
[14] H. Yu, X. Yang, R. Wang, A.G. Fane, Analysis of heat and mass transfer by CFD for performance enhancement in direct contact membrane distillation, J. Membr. Sci., 405–406 (2012) 38–47.
[15] X. Yang, H. Yu, R. Wang, A.G. Fane, Optimization of micro-structured hollow fiber design for membrane distillation applications using CFD modeling, J. Membr. Sci., 421–422 (2012) 258–270.
[16] S. Al-Sharif, M. Albeirutty, A. Cipollina, G. Micale, Modelling flow and heat transfer in spacer-filled membrane distillation channels using open source CFD code, Desalination, 311 (2013) 103–112.
[17] H. Hayer, O. Bakhtiari, T. Mohammadi, Simulation of momentum, heat and mass transfer in direct contact membrane distillation: a computational fluid dynamics approach, J. Ind. Eng. Chem., 21 (2015) 1379–1382.
[18] H. Chang, J.-A. Hsu, C.-L. Chang, C.-D. Ho, CFD simulation of direct contact membrane distillation modules with rough surface channels, Energy Procedia, 75 (2015) 3083–3090.
[19] D. Park, E. Norouzi, C. Park, Experimental and Numerical Study of Water Distillation Performance of Small-Scale Direct Contact Membrane Distillation System, International Mechanical Engineering Congress and Exposition, Heat Transfer Therm. Eng., 8 (2017) 1–9.
[20] S. Soukane, M.W. Naceur, L. Francis, A. Alsaadi, N. Ghaffour, Effect of feed flow pattern on the distribution of permeate fluxes in desalination by direct contact membrane distillation, Desalination, 418 (2017) 43–59.
[21] I. Hitsov, T. Maere, K. De Sitter, C. Dotremont, I. Nopens, Modelling approaches in membrane distillation: a critical review, Sep. Purif. Technol., 142 (2015) 48–64.
[22] L. Francis, N. Ghaffour, A.S. Al-Saadi, G.L. Amy, Submerged membrane distillation for seawater desalination, Desal. Wat. Treat., 55 (2014) 1–6.
[23] M.H. Sharqawy, J.H. Lienhard V, S.M. Zubair, Thermophysical properties of seawater: a review of existing correlations and data, Desal. Wat. Treat., 16 (2013) 1–67.
[24] A.S. Alsaadi, N. Ghaffour, J.-D. Li, S. Gray, L. Francis, H. Maab, G.L. Amy, Modeling of air-gap membrane distillation process: a theoretical and experimental study, J. Membr. Sci., 445 (2013) 53–65.
[25] F.R. Menter, Two-equation eddy-viscosity turbulence models for engineering applications, AIAA J., 32 (1994) 1598–1605.
[26] K.W. Lawson, D.R. Lloyd, Membrane distillation, J. Membr. Sci., 124 (1997) 1–25.
[27] M. Khayet, Membranes and theoretical modeling of membrane distillation: a review, Adv. Colloid Interface Sci., 164 (2011) 56–88.
[28] J. Amigo, R. Urtubia, F. Suárez, Exploring the interactions between hydrodynamics and fouling in membrane distillation systems – a multiscale approach using CFD, Desalination, 444 (2018) 63–74.
[29] A. Alkhudhiri, N. Darwish, N. Hilal, Membrane distillation: a comprehensive review, Desalination, 287 (2012) 2–18.
[30] M. Qtaishat, T. Matsuura, B. Kruczek, M. Khayet, Heat and mass transfer analysis in direct contact membrane distillation, Desalination, 219 (2008) 272–292.
[31] J. Phattaranawik, R. Jiraratananon, A.G. Fane, Effect of pore size distribution and air flux on mass transport in direct contact membrane distillation, J. Membr. Sci., 215 (2003) 75–85.
[32] J. Phattaranawik, R. Jiraratananon, A.G. Fane, Heat transport and membrane distillation coefficients in direct contact membrane distillation, J. Membr. Sci., 212 (2003) 177–193.
[33] A.G. Fane, R.W. Schofield, C.J.D. Fell, The efficient use of energy in membrane distillation, Desalination, 64 (1987) 231–243.
[34] M. Usta, A.E. Anqi, A. Oztekin, Reverse osmosis desalination modules containing corrugated membranes – computational study, Desalination, 416 (2017) 129–139.
[35] A.E. Anqi, M. Usta, M. Alrehili, N. Alkhamis, A. Oztekin, Reverse Osmosis Desalination Module: Three Dimensional, Transient Analyses, International Mechanical Engineering Congress and Exposition, Fluids Eng., 7 (2016) 1–8.
[36] A.M. Alshwairekh, A.A. Alghafis, M. Usta, A.M. Alwatban, R. Krysko, A. Oztekin, The Effect of Porous Support Layer in Forward Osmosis Membranes: A Computational Fluid Dynamics Simulation, International Mechanical Engineering Congress and Exposition, Fluids Eng., 7 (2018) 1–9.
[37] A.E. Anqi, N. Alkhamis, A. Oztekin, Numerical simulation of brackish water desalination by a reverse osmosis membrane, Desalination, 369 (2015) 156–164.
[38] S. Wardeh, H.P. Morvan, CFD simulations of flow and concentration polarization in spacer-filled channels for application to water desalination, Chem. Eng. Res. Des., 86 (2008) 1107–1116.
[39] P. Termpiyakul, R. Jiraratananon, S. Srisurichan, Heat and mass transfer characteristics of a direct contact membrane distillation process for desalination, Desalination, 177 (2005) 133–141.
[40] M. Usta, R.M. Krysco, A.E. Anqi, A. Alshwairekh, A. Oztekin, The Effect of PTFE Membrane Properties on Vacuum Membrane Distillation Module Performance, International Mechanical Engineering Congress and Exposition, Fluids Eng., 7 (2018) 1–8.
[41] M.M.A. Shirazi, A. Kargari, M.J.A. Shirazi, Direct contact membrane distillation for seawater desalination, Desal. Wat. Treat., 49 (2012) 368–375.
[42] K. He, H.J. Hwang, M.W. Woo, I.S. Moon, Production of drinking water from saline water by direct contact membrane distillation (DCMD), J. Ind. Eng. Chem., 17 (2011) 41–48.
[43] M.M.A. Shirazi, A. Kargari, D. Bastani, L. Fatehi, Production of drinking water from seawater using membrane distillation (MD) alternative: direct contact MD and sweeping gas MD approaches, Desal. Wat. Treat., 52 (2014) 2372–2381.
[44] M.M.A. Shirazi, A. Kargari, M. Tabatabaei, Evaluation of commercial PTFE membranes in desalination by direct contact membrane distillation, Chem. Eng. Process. Process Intensif., 76 (2014) 16–25.
[45] A. Boubakri, R. Bouchrit, A. Hafiane, S. Al-Tahar Bouguecha, Fluoride removal from aqueous solution by direct contact membrane distillation: theoretical and experimental studies, Environ. Sci. Pollut. Res., 21 (2014) 10493–10501.
[46] G. Naidu, S. Jeong, S. Vigneswaran, T.-m. Hwang, Y.-J. Choi, S.H. Kim, A review on fouling of membrane distillation, Desal. Wat. Treat., 57 (2016) 10052–10076.
[47] I.S. Al-Mutaz, A.S. Al-Motek, I. Wazeer, Variation of distillate flux in direct contact membrane distillation for water desalination, Desal. Wat. Treat., 62 (2017) 86–93.
[48] A. Luo, N. Lior, Study of advancement to higher temperature membrane distillation, Desalination, 419 (2017) 88–100.